Analytical Methods

Accepted Manuscript

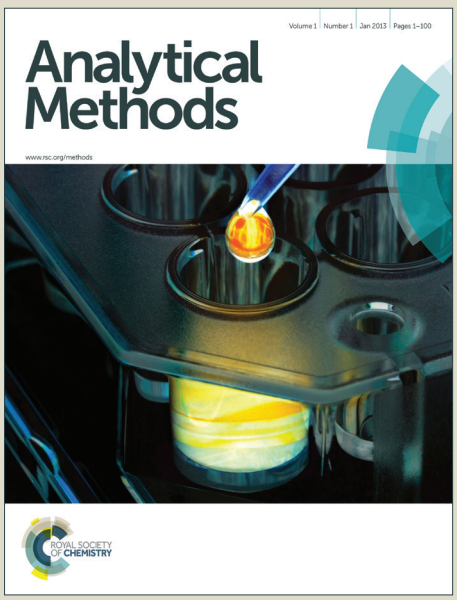

ROYAL SOCIETY OF CHEMISTRY

www.rsc.org/methods

One-step green synthesis of polypyrrole-Au nanocomposite and its application in myoglobin aptasensor

Chong Sun[a], Daoying Wang*[,a] , Zhiming Geng[a], Ling Gao[b], Muhan Zhang[a], Huan Bian[a], Fang Liu[a], Yongzhi Zhu[a], Haihong Wu[a], Weimin Xu*[,a]

[a]*Institute of Agricultural Products Processing, Jiangsu Academy of Agricultural Sciences, Nanjing 210014, China*

[b]*Jiangsu Collaborative Innovation Center of Biomedical Functional Materials, College of Chemistry and Materials Science, Nanjing Normal University, Nanjing 210023, China*

*Corresponding author.

E-mail address: daoyingwang@yahoo.com (D. Wang); weiminxu2002@aliyun.com (W. Xu)

Tel.: +86 25 84390065, Fax: +86 25 84390065

Abstract:

An electrochemical aptasensor was fabricated based on polypyrrole-Au nanocomposite (PPy-Au NC) and myoglobin-binding aptamer (MBA). The PPy-Au NC was synthesized using one-step green synthesis method, and was characterized by transmission electron microscopy (TEM), UV-*vis* spectroscopy and diffuse reflectance spectrum. Studies revealed the PPy-Au NC provided mild micro-environment and large surface area for MBA immobilization and facilitated electron transfer. The glassy carbon electrodes (GCEs) surface modified with PPy-Au NC was grafted with MBA, which had excellent binding affinity and selectivity for myoglobin (Mb). Binding of the Mb at the modified GCE surface greatly restrained access of electrons for a redox probe of $[Fe(CN)_6]^{3-/4-}$. Moreover, the aptasensor could

be used for detection of Mb in biochemical assays, with a wide detection range (0.0001 to 0.15 $g \cdot L^{-1}$) and a low detection limit of 30.9 $ng \cdot mL^{-1}$. The aptasensor had a good anti-interference property towards hemin, glucose oxidase (GOx), cytochrome c and hemoglobin. The idea and method will provide a new approach for evaluation of freshness and quality of stored meat.

Keywords: Electrochemical aptasensor; Green synthesis method; Polypyrrole-Au nanocomposite; Myoglobin detection

1. Introduction

Myoglobin (Mb), which is comprised of a folded polypeptides portion, globin and an iron- porphyrin-containing prosthetic group, is mainly found in the muscular tissues and responsible for transport and storage of molecular oxygen by reversibly binding with it [1]. In addition, Mb can also transport fatty acids through the muscle cell cytoplasm [2]. In food industry, Mb is predominantly linked to color of muscular tissues. During storage, meat gets darker due to chemical changes of Mb. Thus, the variation in Mb content and structure is related to freshness and storage quality, which is essential in evaluating quality of meat [3-6].

At present, the main methods for detection of Mb are colorimetric method and immunoassay. Colorimetric method is based on iron valence of iron porphyrin in Mb. As we all know, hemoglobin is similar to Mb in terms of the structure, which can

interfere the colorimetric determination of Mb. Meanwhile, antibodies used in immunoassay are usually very expensive, and they should be stored at strictly low temperature [1]. Aptamers are artificial oligonucleic acids to bind specific target molecules, which are *in vitro* selected by SELEX (systematic evolution of ligands by exponential enrichment) technology [7,8]. Theoretically, it is possible to obtain all kinds of aptamers to recognize virtually different target molecules with high affinity and specificity. Aptamers used for specific protein binding studies have drawn much attention recently [9-14]. To overcome the constraints of immunoassay and take advantage of the electrochemical technique and aptamers, we developed a label-free electrochemical aptasensor for the detection of Mb in this paper.

Nowadays, conducting polymers have been the subject of much interest, not only from a fundamental scientific interest but also from a practical point of view, such as various functional applications including solar cells, separation membrane, molecular electronic devices and biosensing devices. Among the class of applications, biosensors take up the running due to the inherent charge transport properties and biocompatibility of the conducting polymer [15-19]. However, for the preparation of PPy nanoparticles with specific functional groups, polymers possessing such functionality need to be synthesized through complicated routes or post-functionalization of the PPy nanoparticles with the moiety of interest. Au nanoparticles (Au NPs) become widely used recently because of their excellent biocompatibility and functionality [20-31]. In this case, polypyrrole-Au nanocomposite (PPy-Au NC) was designed and synthesized using a green process. In

the process of preparation of PPy-Au NC, $HAuCl_4 \cdot 3H_2O$ was used as oxidant and Au was doped into PPy-Au NC. The PPy-Au NC was expected to present all the advantageous properties of the two kinds of materials. Subsequently, the PPy-Au NC was immobilized on the surface of glass carbon electrode (GCE) and a label-free electrochemical aptasensor using myoglobin-binding aptamer (MBA) as receptor was developed for the measurement of Mb. More details in the preparation of electrode that modified by PPy-Au NC, and the electrochemical detection and analysis of Mb were presented.

2. Experiments section

2.1. Reagents and instruments

Mb was obtained from Sigma-Aldrich (USA), hydrogen tetrachloroaurate (III) trihydrate ($HAuCl_4 \cdot 3H_2O$, 99.9%) was obtained from Alfa Aesar, a Johnson Matthey Company and pyrrole (99%) was received from ACROS Organics Co., Ltd. (USA). MBA was purchased from Sangon Biotechnology Co., Ltd. (China) with HPLC purification. The 5'-terminus of MBA contained 40 bases with its sequence as follows: 5'-NH_2-CCCTCCTTTCCTTCGACGTAGATCTGCTGCGTTGTTCCGA-3'. All reagents were of analytic grade and used as received. Phosphate buffer solution (PBS) was prepared by mixing stock standard solution of NaCl, KCl, Na_2HPO_4 and KH_2PO_4. Double-distilled water was used throughout.

2.2. Preparation of PPy-Au NC

A green process for preparing PPy-Au NC was described as follows. 100 μL of pyrrole agent was added into 30 mL of 0.05% $HAuCl_4 \cdot 3H_2O$ slowly under 0~5 ℃ ice water bath condition. The mixed solution was stirred for 6 h to obtain the PPy-Au NC, and the color of solution turned into atropurpureus. In the process, $HAuCl_4 \cdot 3H_2O$ and pyrrole were used as oxidant and reductant respectively. The product was dialyzed with Spectra/Por CE (MWCO = 14400) in water to thoroughly remove excessive Au^{3+}. The resulting PPy-Au NC was used for characterization and detection.

2.3. Characterization of PPy-Au NC and MBA/(PPy-Au) hybrids

The morphology of the PPy-Au NC was characterized by transmission electron microscopy (TEM) that carried out with HITACHI H-7650 (Hitachi, Japan). Specimens for inspection were prepared on a 200 mesh copper grid by slowly evaporating one drop of prepared solutions covered by a carbon-supported film at room temperature. The size and Zeta Potential (ζ) of the PPy-Au NC was detected using a Nano ZS90 Zetasizer (Malvern Instruments, UK). The measurements were made in automatic mode, and the data were analyzed using the software supplied by the manufacturer. The existence of PPy-Au NC was detected by Cary 50 UV-*vis* spectrophotometer (Varian Co., USA). Diffuse reflectance spectrum was obtained with a Cary 5000 spectrophotometer and samples were dropped on the cleaned quartz plates for characterization (Varian Co., USA). The circular dichroism (CD) spectra were collected from 185 to 280 nm at 1.0 nm intervals on an Applied Photophysics Chriascan circular dichroism spectrometer using a quartz cell with a path length of 1 cm at room temperature. Each spectrum was accumulated in triplicate and the

obtained results were expressed as millidegrees (mdeg).

2.4. Preparation and measurement of the aptasensor

Prior to modification, GCE (diameter of 3 mm) was polished with 0.3 and 0.05 μm alumina slurry, respectively, and rinsed thoroughly with double-distilled water between each polishing step. The electrodes were successively sonicated in ethanol and double-distilled water, and then allowed to dry at room temperature. The modification process of the electrodes was shown in Scheme 1. 8 μL of 0.1% APTES ethanol solution was dropped onto the surface of GCE and dried under the infrared lamp. APTES was linked to the GCE surface through the silicon-oxygen bonds. Then, 8.0 μL of the PPy-Au NC was dropped onto the pretreated electrode surface and dried in air. PPy-Au NC was immobilized *via* Au combined with the amino at the end of APTES molecule. After that, MBA was molecularly grafted onto the surface of modified GCE *via* Au combined with the amino at the end of MBA molecule. In the presence of the target molecule of Mb, a complex was formed and such a complex increased the steric hindrance that greatly restrained access of electrons for a redox probe of $[Fe(CN)_6]^{3-/4-}$. When not in use, the electrodes were stored at 4 ºC in a refrigerator.

All electrochemical measurements were performed with a CHI 660D workstation (Shanghai, China). A three-electrode system comprised of the modified GCE as working electrode, a platinum wire as auxiliary electrode and a saturated calomel electrode (SCE) as reference electrode was employed for all electrochemical experiments. All the potentials given here were relative to SCE. Cyclic

voltammograms (CVs) were performed in the potential between -0.2 and 0.7 V, while differential pulse voltammetry (DPV) was recorded under the condition: pulse amplitude of 50 mV, pulse width of 50 ms and voltage ranging from -0.2 to 0.7 V. The electrochemical impedance spectroscopy (EIS) tests were carried out in AC voltage amplitude 5 mV, frequency range 1 to 10 kHz, and open circuit potential.

2.5. Mb determination in muscles

Mb was exacted according to the method described as follows: 2 g muscles were homogenized in 20 mL 0.04 M PBS (pH=6.8) at 10800 $r \cdot min^{-1}$ for 25 s with an Ultra Turrax (T25, IKA, Germany), then the homogenate was put into ice-water bath for 1 h. After that, the homogenate was centrifuged for 30 min at 10000 *g* at 10~15 ℃ (Allegra 64R, Beckman, USA). Then the supernatant was collected and diluted with buffer for the biochemical assay.

The control experiment employed to detect Mb by colorimetry was conducted according to the literature [32]. For the determination of Mb, the absorbancies of the extracts were measured at 572 nm, 565 nm, 545 nm and 525 nm and the total concentrations of Mb were calculated using the following formula [32].

$$Total_{Mb}\ (mM) = (-0.166A_{572}) + 0.086\ A_{565} + 0.088\ A_{545} + 0.099\ A_{525}$$

3. Results and discussion

3.1. Characterization of the PPy-Au NC

TEM was performed to estimate the size and morphology of the PPy-Au NC. Typical TEM photograph showed that PPy-Au NC had been well dispersed with an

average diameter of 180 nm (Fig. 1A). Such result was in agreement with the particle size distribution measured by a Zetasizer Nano ZS90 dynamic light scattering all for three analyses (194.5±1.22 nm in diameter, Fig. 1B). As shown in Fig. S1, PPy nanoparticles were precipitated obviously (Fig. S1A). However, PPy-Au NC were dispersed in aqoeous solution excellently, which should be attributed to the fact that Au acted as dopant (Fig. S1B). UV-*vis* absorption spectra were used to confirm the successful binding of PPy-Au NC. As shown in Fig. S2, Au showed an absorption peak from 500 to 600 nm [33]. Meanwhile, an absorption peak appeared at about 460 nm was a characteristic of PPy [34-36], indicating the successful binding between Au and PPy.

3.2. Characterization of MBA/(PPy-Au) hybrids

Fig. 2 showed the diffuse reflectance spectrum of MBA/(PPy-Au) hybrids, where three peaks were observed during the process. The peaks at 610 nm and 460 nm were attributed to Au and PPy, indicating the successful binding between Au and PPy. After MBA was attached to PPy-Au NC, an obvious absorption peak appeared at 364 nm that was shown in Fig. 2, which was a characteristic of the DNA strand, indicating the successful binding between MBA and PPy-Au NC.

To validate the conformational change of binding interaction, we measured the CD spectra of MBA under different conditions. It is reported that CD can measure the structures and ligand binding of quadruplex DNAs [10,37]. Therefore we investigated the conformation change of MBA after the addition of Mb (Fig. 3). Upon the addition of PPy-Au NC, the characteristic peaks were similar to those of the pure MBA (curve

a) in both peak intensity and peak position (curve b). In the presence of 1 μL 0.05 $g \cdot L^{-1}$ Mb, the positive peak increased and shifted to about 191 nm and 195 nm (curve c). With the increasing of Mb concentrations to 10 μL, the positive peak continued to rise in CD spectra (curve d), indicating formation of the MBA quadruplex. The results suggested that the G-quadruplex structure of MBA was induced by specific interaction between MBA and Mb [38]. Thus, PPy-Au NC were crucial for the conformational conversion of aptamer (i.e. change of a single strand in helix conformation to the G-quadruplex form), which is attributed to the good biocompatibility of nanocomposite.

3.3. Optimization of the MBA/(PPy-Au) aptasensor

The sensitivity of the aptasensor is often affected by some factors, such as pH value of buffer solution, temperature and interaction time of MBA and Mb. These factors were optimized when the aptasensor was incubated in 0.05 $g \cdot L^{-1}$ Mb.

The pH value had a great effect on the electrochemical response of the aptasensor [39]. The pH value ranging from 3.0 to 8.0 was adopted in this study. As shown in Fig. 4A, compared to the data of response currents obtained at other pH values, much larger response current was obtained within the pH ranging from 5.0 to 6.0. The normal pH values of pork muscles are between 6.0 and 6.4 [40]. Thus, the buffer solution was adjusted to pH 6.0 and used in all experiments below.

Fig. 4B showed the effect of temperature on the response current of the aptasensor. The current was increased with increasing temperature to 30 °C and then it was decreased. Therefore, 30 °C was chosen as the optimal temperature.

Since the interaction of MBA and Mb is dependent on incubation time, the effect of incubation time on biosensor response was studied. Fig. 4C showed the dependence of current on incubation time. Binding of the Mb at the modified GCE surface greatly restrained access of electrons for a redox probe of $[Fe(CN)_6]^{3-/4-}$. The plot in Fig. 4C suggested that the current response decreased with the incubation time from 0 to 100 min and reached a plateau after 80 min, suggesting that the binding between MBA and Mb almost reached saturation at 80 min. Thus, 80 min was chosen as the incubation time for the following experiments.

3.4. Effect of scan rate

CV was used to study the MBA/(PPy-Au)/APTES/GCE behavior in 0.1 M PBS (pH=6.0) containing 10 mM $[Fe(CN)_6]^{3-/4-}$(1:1) solution and 0.1 M KCl. Both redox peak currents enlarged gradually with the increasing scan rate (Fig. S3). The reduction and oxidation peak currents were linearly proportional to the scan rate ranging from 20 to 120 $mV \cdot s^{-1}$ with the results of I_{pa} (μA) = 3.8144 + 54.00 υ ($mV \cdot s^{-1}$) (r = 0.9915) and I_{pc} (μA) = -3.4548 – 53.44 υ ($mV \cdot s^{-1}$) (r = 0.9953). The increase in peak currents with the scan rate, maintaining a constant potential, suggested the occurrence of surface confined and reversible diffusion had less redox transitions within the MBA/(PPy-Au)/APTES/GCE [41].

3.5. Electrochemical characteristics of the MBA/(PPy-Au) aptasensor

CVs were used to evaluate the changes of electrode behavior after each modified step [42-44]. As shown in Fig. 5A, the PPy-Au NC modified GCE resulted in higher background current (curve a), due to the good conductivity of PPy-Au NC. When

MBA was grafted onto the (PPy-Au)/APTES/GCE, the modified electrode exhibited a pair of stable and well-defined redox peaks at 0.350 and 0.152 V in 0.1 M PBS (pH = 6.0) containing 10 mM $[Fe(CN)_6]^{3-/4-}$(1:1) solution and 0.1 M KCl (curve b), which corresponded to the formation of an organic layer of MBA [10]. Upon incubation with Mb solution, the peak current decreased greatly, suggesting an obvious steric hindrance process for the binding of Mb to the surface of the modified GCE (curve c). Comparing MBA/(PPy-Au)/APTES/GCE (insert of Fig. 5A, black line) with MBA modified GCE (insert of Fig. 5A, red line), we found that the structure of PPy-Au NC can provide high surface to volume ratios and high surface activity, thus it possessed advantages in terms of MBA immobilization. As shown in Fig. S4, the background current of MBA/(PPy-Au)/APTES/GCE (curve a) was much higher than MBA/Au/APTES/GCE (curve b) because of the good conductivity of PPy-Au NC. While incubation with Mb solution, the peak currents of Mb/MBA/(PPy-Au)/APTES/GCE (curve c) and Mb/MBA/Au/APTES/GCE (curve d) decreased greatly for the nonconduction of Mb. Meanwhile, the separation of peak potentials (ΔEp) of Mb/MBA/(PPy-Au)/APTES/GCE was 157 mV, while Mb/MBA/Au/APTES/GCE was 302 mV. The results indicated Mb attached to the MBA/Au/APTES/GCE surface had more spatial freedom in its orientation, which made it much easier for the electroactive center of Mb to unfold [45]. Thus, it was possible to facilitate and achieve fast direct electron transfer between the heme site of immobilized Mb and the electrode surface.

For further characterization of the different modified electrodes, the

electrochemical impedance spectroscopy (EIS) was used in the frequency ranging from 1 Hz to 10 kHz at a formal potential value ($E^{0'}$) of 0.251 V vs. SCE. As we know, the semi-circle diameter in EIS equals the interface electron-transfer resistance (R_{et}), which controls the electron-transfer kinetics of the redox probe at the electrode interface. Fig. S5 illustrated the typical Nyquist diagram at the (PPy-Au)/APTES/GCE (a), MBA/(PPy-Au)/APTES/GCE (b) and Mb/MBA/(PPy-Au)/APTES/GCE (c) in 10 mM $[Fe(CN)_6]^{3-/4-}$(1:1) solution containing 0.1 M KCl. The (PPy-Au)/APTES/GCE decreased the R_{et} tremendously, because PPy and Au can improve the conductivity of the GCE and facilitate the electron transfer between solution and electrode interface. A bigger well-defined semi-circle at high frequency regions was observed at MBA/(PPy-Au)/APTES/GCE compared with the (PPy-Au)/APTES/GCE, indicating that the non-conductivity of MBA inhibited the electron transfer of the redox probe of $[Fe(CN)_6]^{3-/4-}$ to the electrode surface to some degree. When Mb was assembled on the MBA/(PPy-Au)/APTES/GCE, the resistance increased greatly, owing to the fact that the dielectric behavior of Mb for interfacial electron transfer processes and it blocked the electron exchange between the redox probe and the electrode. Thus, we can conclude that the PPy-Au film not only offer a biocompatible surface for protein loading and protein capture but also provide a sensitive electric interface for further sensing.

Fig. 5B and C displayed the DPVs for the determination of Mb, where the linear concentration ranges were obtained from 0.0001 to 0.15 $g \cdot L^{-1}$ with a correlation

coefficient (R^2) of 0.9931 (n = 10). The linear regression equation was I (μA) = -104.12 c + 18.02, where I was current and c was the Mb concentration. The limit of detection was estimated from the equation: LOD = 3σ/κ as 30.9 ng·mL^{-1} with the signal to noise ratio being 3. In the above equation, σ is the standard deviation of the blank solution (i.e. without Mb) and κ denotes the slope of the calibration curve (Fig. 5C). Moreover, an analytical performance comparison of some determination methods reported by previous papers and the novel aptasensor we prepared was performed. From Table S1, the proposed aptasensor showed a better linearity in a wider range and a lower detection limit than those previous reported models [46-49], which were attributed to the high surface to volume ratios and high surface activity of the PPy-Au NC to immobilize MBA.

The stability of the aptasensors was evaluated over a period of 30 days of storage (at 4 ºC). After two weeks and four weeks, the aptasensors retained 96.8% and 95.4% of the initial response respectively. The reproducibility of the as-prepared aptasensors was investigated with intra-assay progress. Five paralled electrodes were prepared to analyze the same concentration of Mb (0.05 g·L^{-1}) resulted in a relative standard deviation (R.S.D.) of 4.6%. These results indicated that the aptasensor had a good stability and reproducibility.

3.6. Effect of interfering substances

The measurement of Mb affected by various possible interfering substances found in muscle such as hemin, glucose oxidase (GOx), cytochrome c and hemoglobin was carried out [50]. The effect of all these compounds was checked carrying out DPV

measurements in 10 mM $[Fe(CN)_6]^{3-/4-}$(1:1) solution containing 0.1 M KCl with a concentration of 5 $g \cdot L^{-1}$ of each compound and compared with the results that obtained with 0.05 $g \cdot L^{-1}$ Mb alone. As seen from Fig. S6, the aptasensor showed little response to the interfering substances and no apparent difference in current upon addition of these compounds, which was attributed to Mb specific binding to MBA.

3.7. Analysis of real samples

As the subject of applicability in practical analysis, four muscles were analyzed separately by the aptasensor and colorimetry as a reference method (Table S2), and the results obtained were compared in order to validate its performance. Colorimetry is not specific and less sensitive, which is influenced by many factors such as pH, temperature, salinity, hemoglobin and so on. It showed that the values measured by the aptasensor were lower than the data determined by colorimetry because of the greater specificity of the aptasensor. Thus, the values we measured with the aptasensor were much close to the real values. The results showed the applicability of the biosensor for determination of the concentration of Mb in practical samples.

4. Conclusion

The development of polymer nanocomposites has considerable effects on biochemical assays. In this paper, the novel PPy-Au NC with conductivity and biocompatibility was synthesized using one-step green synthesis method, and then a sensitive aptasensor based on the PPy-Au NC was prepared and applied in the analysis of Mb in practical samples. The aptasensor exhibited a low detection limit

of 30.9 ng·mL^{-1}, a wide concentration ranging from 0.0001 to 0.15 g·L^{-1}, and good anti-interference property. The structure of PPy-Au NC could provide high surface to volume ratios and high surface activity, thus it possessed advantages in terms of MBA immobilization, which ensured that Mb would be covalently linked to GCE. This method proposed a great potential especially for evaluation of meat freshness and storage quality.

Acknowledgments

This work was supported by National Natural Science Foundation of China (31271891), Natural Science Foundation Program of Jiangsu Province (BK2012785).

Appendix A. Supplementary material

References

1 S.S. Mandal, K.K. Narayan and A.J. Bhattacharyya, *J. Mater. Chem. B*, 2013, **1**, 3051-3056.

2 B.A. Wittenberg, J.B. Witteaberg and P.R. Caldwell, *J. Biol. Chem.*, 1975, **250**, 9038-9043.

3 J.B. Fox, in *The Science of Meat and Meat Products*, ed. J.F. Price and B.S. Schweigert, Food and Nutrition Press, Westport, 3nd edn., 1987, pp. 193-215.

4 D.J. Livingston and W.D. Brown, *Food Technol.*, 1981, **35**, 244-252.

5 J.B. Jr. Fox, J. Agr. *Food Chem.*, 1966, **14**, 207-210.

6 R.W. Kranen, T.H. Vankuppelvelt, H.A. Goedhart, C.H. Veerkamp, E. Lamboy and

J.H. Veerkamp, *Poultry Sci.*, 1999, **78**, 467-476.

7 T. Hermann and D.J. Patel, *Science*, 2000, **287**, 820-825.

8 E. Luzi, M. Minunni, S. Tombelli and M. Mascini, *Trends Anal. Chem.*, 2003, **22**, 810-818.

9 A. Bourdoncle, A. Estevez, C. Gosse, L. Lacroix, P. Vekhoff, L.T. Saux, L. Jullien and J.L. Mergny, *J. Am. Chem. Soc.*, 2006, **128**, 11094-11105.

10 G.S. Bang, S. Cho and B.G. Kim, *Biosens. Bioelectron.*, 2005, **21**, 863-870.

11 S.H. Chou, K.H. Chin and A.H. Wang, *Trends Biochem. Sci.*, 2005, **30**, 231-234.

12 F.L. Floch, H.A. Ho and M. Leclerc, *Anal. Chem.*, 2006, **78**, 4727-4731.

13 M. Zayats, Y. Huang, R. Gill, C.A. Ma and I. Willner, *J. Am. Chem. Soc.*, 2006, **128**, 13666-13667.

14 J.J. Li, Y. Chu, B.Y. Lee and X.S. Xie, *Nucleic Acids Res.*, 2008, **36**, e36.

15 C.M. Hangarter, M. Bangar, A. Mulchandani and N.V. Myung, *J. Mater. Chem.*, 2010, **20**, 3131-3140.

16 A.G. Elie, *Biomaterials*, 2010, **31**, 2701-2716.

17 J.L.G. Alvarez, *Curr. Org. Chem.*, 2008, **12**, 1199-1219.

18 T. Yamamoto, H. Fukumoto and T. Koizumi, *J. Inorg. Organomet. Polym.*, 2009, **19**, 3-11.

19 L. Dai, P. Soundarrajan and T. Kim, *Pure Appl. Chem.*, 2002, **74**, 1753-1772.

20 M. Hu, J.Y. Chen, Z.Y. Li, L. Au, G.V. Hartland, X.D. Li, M. Marquez and Y.N. Xia, *Chem. Soc. Rev.*, 2006, **35**, 1084-1094.

21 M.C. Daniel and D. Astruc, *Chem. Rev.*, 2004, **104**, 293-346.

22 S. Li, H. Liu, L. Liu, L. Tian and N. He, *Anal. Biochem.*, 2010, **405**, 141-143.

23 H. Liu, S. Li, L. Liu, L. Tian and N. He, *Biosens. Bioelectron.*, 2010, **26**, 1442-1448.

24 C.M. Cobley, J.Y. Chen, E.C. Cho, L.V. Wang and Y.N. Xia, *Chem. Soc. Rev.*, 2011, **40**, 44-56.

25 M.M. Shenoi, N.B. Shah, R.J. Griffin, G.M. Vercellotti and J.C. Bischof, *Nanomedicine*, 2011, **6**, 545-563.

26 V. Pokharkar, D. Bhumkar, K. Suresh, Y. Shinde, S. Gairola and S.S. Jadhav, *J. Biomed. Nanotechnol.*, 2011, **7**, 57-59.

27 S. Maiti, *J. Biomed. Nanotechnol.*, 2011, **7**, 65.

28 D.K. Kim, S.J. Park, J.H. Lee, Y.Y. Jeong and S.Y. Jon, *J. Am. Chem. Soc.*, 2007, **129**, 7661-7665.

29 S.E. Skrabalak, J. Chen, L. Au, X. Lu, X. Li and Y. Xia, *Adv. Mater.*, 2007, **19**, 3177-3184.

30 J.Y. Chen, M.X. Yang, Q.A. Zhang, E.C. Cho, C.M. Cobley, C. Kim, C.L. Glaus, H.V. Wang, M.J. Welch and Y.N. Xia, *Adv. Funct. Mater.*, 2010, **20**, 3684-3694.

31 C. Alric, J. Taleb, G.L. Duc, C. Mandon, C. Billotey, A.L. Herland, T. Brochard, F. Vocanson, M. Janier, P. Perriat, S. Roux and O. Tillement, *J. Am. Chem. Soc.*, 2008, **130**, 5908-5915.

32 K. Krzywicki, *Meat Sci.*, 1982, **7**, 29-36.

33 Q. Wei, K. Su, S. Durant and X. Zhang, *Nano. Lett.*, 2004, **4**, 1067-1071.

34 M. Chougule, S. Pawar and P. Godse, *Soft Nanosci. Lett.*, 2011, **1**, 6-10.

35 Z. Wang, X. Kong and Y. Ding, *Adv. Funct. Mater.*, 2004, **14**, 943-956.

36 H. Shiigi, M. Kishimoto and H. Yakabe, *Anal. Sci.*, 2002, **18**, 41-44.

37 B.I. Kankia and L.A. Marky, *J. Am. Chem. Soc.*, 2001, **123**, 10799-10804.

38 W. Fei, Y. Zhang, X. Sun, Y. Zhang, H. Cao, H. Shen and N. Jia, *J. Electroanal. Chem.*, 2012, **675**, 5-10.

39 F. Kong, M. Xu, J. Xu and H. Chen, *Talanta*, 2011, **85**, 2620-2625.

40 M. Zhang, D. Wang, Z. Geng, H. Bian, F. Liu, Y. Zhu and W. Xu, *Food Chem.*, 2014, **165**, 337-341.

41 S. Radhakrishnan, C. Sumathi, A. Umar, S.J. Kim, J. Wilson and V. Dharuman, *Biosens. Bioelectron.*, 2013, **47**, 133-140.

42 S. Bharathi, M. Nogami and S. Ikeda, *Langmuir*, 2001, **17**, 1-4.

43 J. Jia, B. Wang, A. Wu, G. Cheng, Z. Li and S. Dong, *Anal. Chem.*, 2002, **74**, 2217-2223.

44 R. Liang, J. Qiu and P. Cai, *Anal. Chim. Acta*, 2005, **534**, 223-229.

45 G.H. Zhang, N.B. Yang, Y.L. Ni, J. Shen, W.B. Zhao and X.H. Huang, *Sensor Actuat. B*, 2011, **158**, 130-137.

46 B. Osman, L. Uzun, N. Beşirli and A. Denizli, *Mater. Sci. Eng. C*, 2013, **33**, 3609-3614.

47 F.T.C. Moreira, R.A.F. Dutra, J.P.C. Noronha and M.G.F. Sales, *Electrochim. Acta*, 2013, **107**, 481-487.

48 S.S. Mandal, K.K.Narayan and A.J. Bhattacharyya, *J. Mater. Chem. B*, 2013, **1**, 3051-3056.

49 D.H. Kim, S.M. Seo, H.M. Cho, S.J. Hong, D.S. Lim and S.H. Paek, *Biosens. Bioelectron.*, 2014, **62**, 234-241.

50 J. Ye and R.P. Baldwin, *Anal. Chem.*, 1988, **60**, 2263-2268

Legends for the figures:

Scheme 1. The modification process of the Mb/MBA/(PPy-Au)/APTES/GCE.

Fig. 1. (A) TEM image of the PPy-Au NC, (B) Particle size distribution of the PPy-Au NC measured by a Zetasizer Nano ZS90 dynamic light scattering.

Fig. 2. Diffusion reflectance spectrum of MBA/(PPy-Au) hybrids.

Fig. 3. CD spectra of (a) MBA, (b) MBA/(PPy-Au), (c) MBA/(PPy-Au) with 1 μL 0.05 $g \cdot L^{-1}$ Mb and (d) MBA/(PPy-Au) with 10 μL 0.05 $g \cdot L^{-1}$ Mb. Scan speed: 50 $nm \cdot min^{-1}$, scan range: 185-280 nm.

Fig. 4. Effects of (A) pH of detection solution, (B) temperature, and (C) incubation time on the peak current. One parameter changed while the others were under their optimal conditions and 0.05 $g \cdot L^{-1}$ Mb was used as an example.

Fig. 5. (A) CVs of (a) PPy-Au NC modified GCE, (b) MBA/(PPy-Au) modified GCE and (c) Mb/MBA/(PPy-Au) modified GCE. The insert was the CVs of MBA/(PPy-Au) modified GCE (black line), and MBA modified GCE (red line). Scan rate: 100 $mV \cdot s^{-1}$. (B) The concentration of Mb was (a) 0, (b) 0.0001 $g \cdot L^{-1}$, (c) 0.0009 $g \cdot L^{-1}$, (d) 0.005 $g \cdot L^{-1}$, (e) 0.009 $g \cdot L^{-1}$, (f) 0.02 $g \cdot L^{-1}$, (g) 0.05 $g \cdot L^{-1}$, (h) 0.09 $g \cdot L^{-1}$ and (i) 0.15 $g \cdot L^{-1}$. (C) The calibration curve between the current response and Mb concentration. The electrolyte: 0.1 M PBS (pH = 6.0) containing 10 mM $[Fe(CN)6]^{3-/4-}$(1:1) solution and 0.1 M KCl.

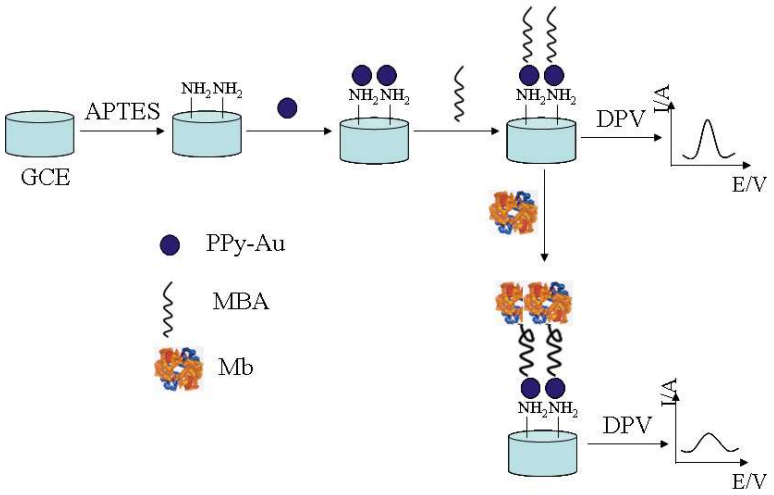

Scheme 1. The modification process of the Mb/MBA/(PPy-Au)/APTES/GCE.

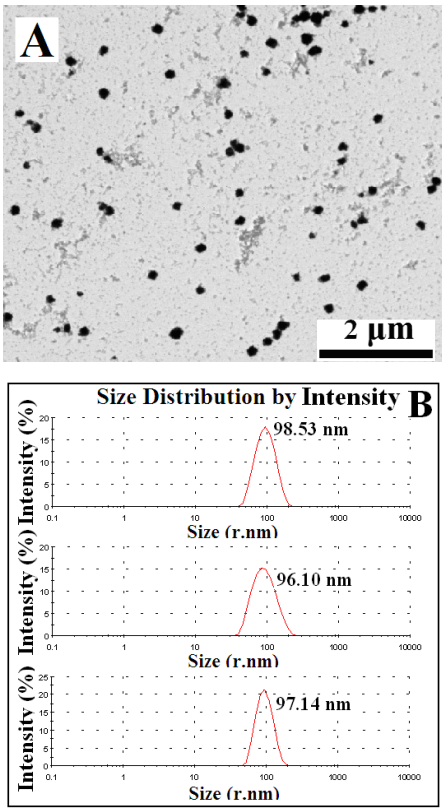

Fig. 1. (A) TEM image of the PPy-Au NC, (B) Particle size distribution of the PPy-Au NC measured by a Zetasizer Nano ZS90 dynamic light scattering.

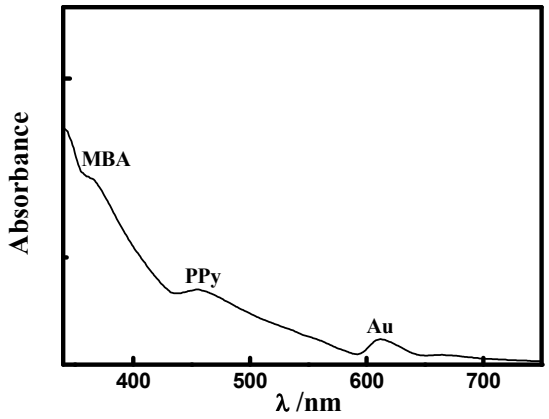

Fig. 2. Diffusion reflectance spectrum of MBA/(PPy-Au) hybrids.

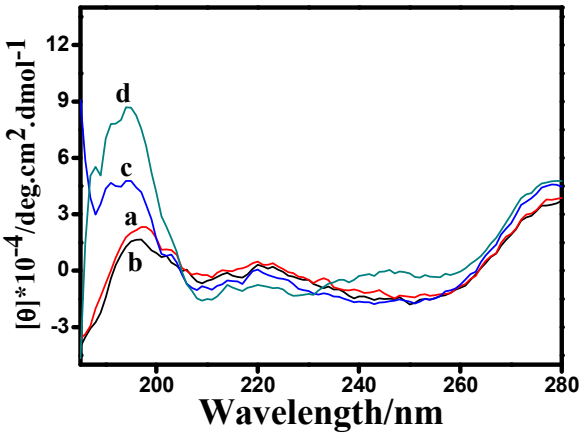

Fig. 3. CD spectra of (a) MBA, (b) MBA/(PPy-Au), (c) MBA/(PPy-Au) with 1 μL 0.05 g·L^{-1} Mb and (d) MBA/(PPy-Au) with 10 μL 0.05 g·L^{-1} Mb. Scan speed: 50 nm·min^{-1}, scan range: 185-280 nm.

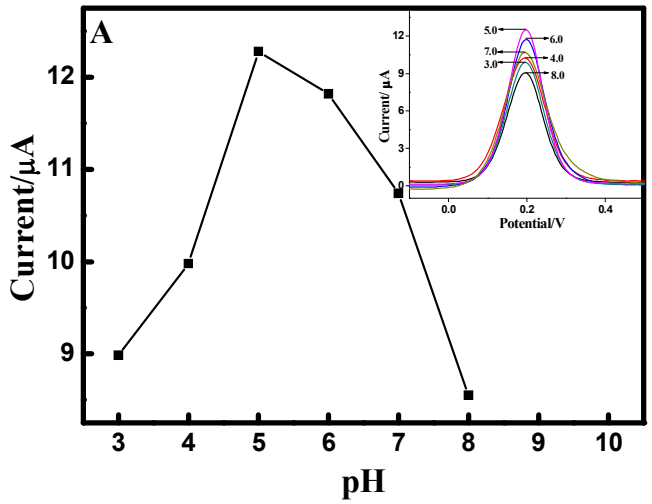

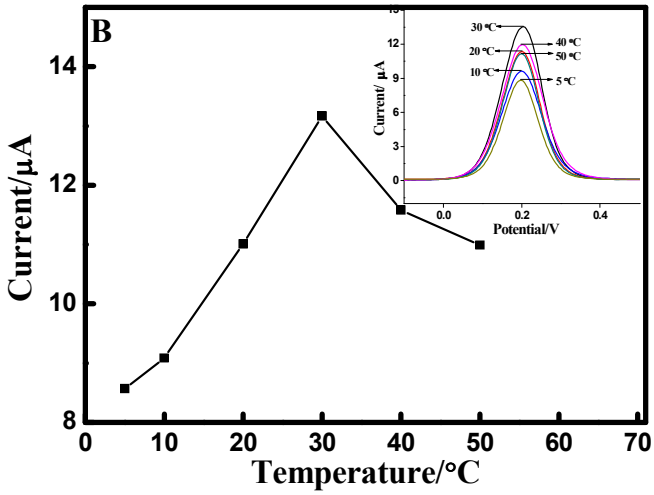

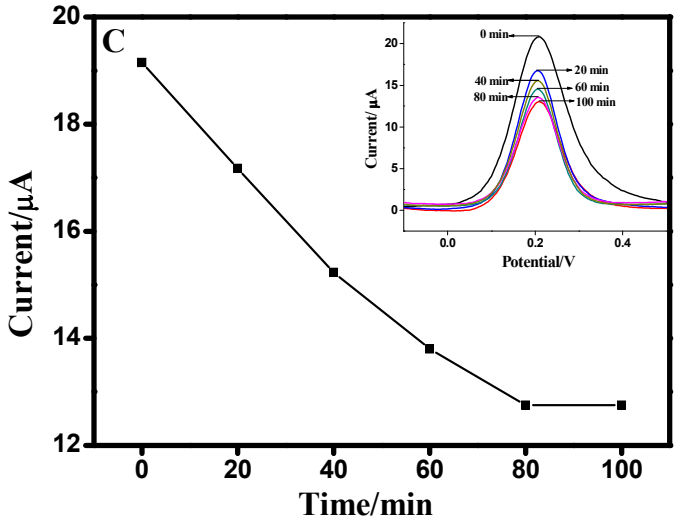

Fig. 4. Effects of (A) pH of detection solution, (B) temperature, and (C) incubation time on the peak current. One parameter changed while the others were under their optimal conditions and 0.05 $g \cdot L^{-1}$ Mb was used as an example.

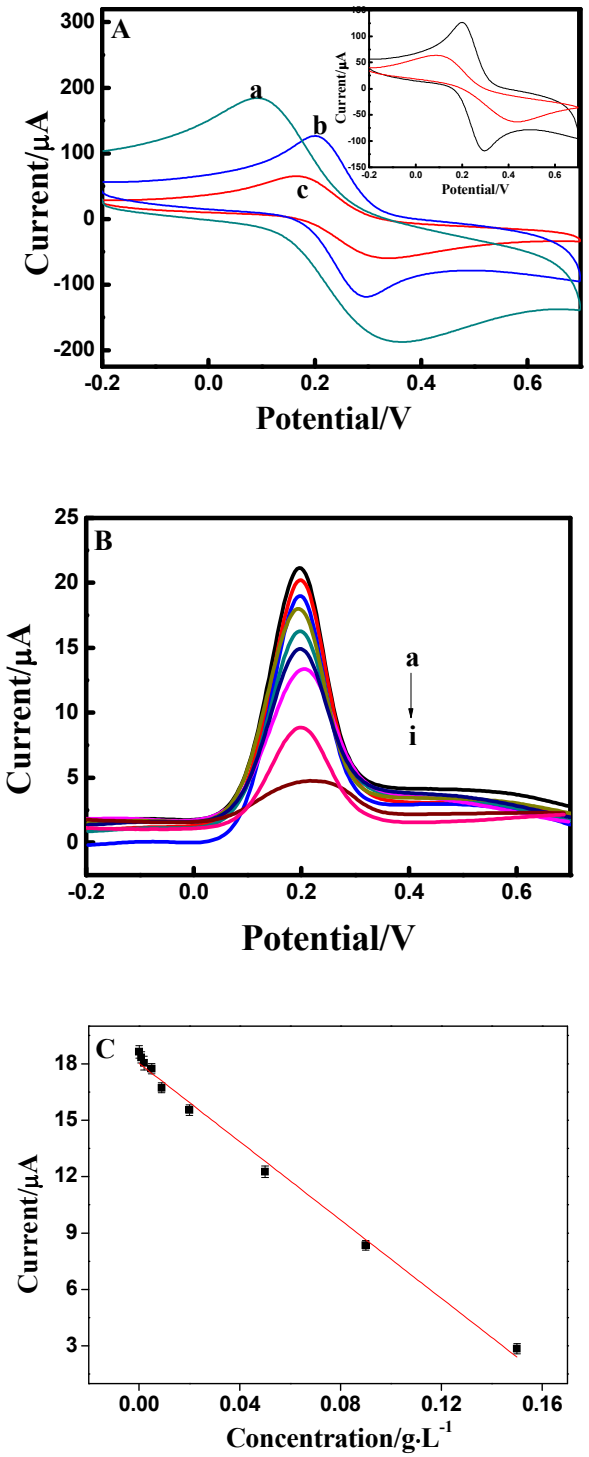

Fig. 5. (A) CVs of (a) PPy-Au NC modified GCE, (b) MBA/(PPy-Au) modified GCE and (c) Mb/MBA/(PPy-Au) modified GCE. The insert was the CVs of MBA/(PPy-Au) modified GCE (black line), and MBA modified GCE (red line). Scan rate: 100 $mV \cdot s^{-1}$. (B) The concentration of Mb was (a) 0, (b) 0.0001 $g \cdot L^{-1}$, (c) 0.0009 $g \cdot L^{-1}$, (d) 0.005

g·L^{-1}, (e) 0.009 g·L^{-1}, (f) 0.02 g·L^{-1}, (g) 0.05 g·L^{-1}, (h) 0.09 g·L^{-1} and (i) 0.15 g·L^{-1}. (C) The calibration curve between the current response and Mb concentration. The electrolyte: 0.1 M PBS (pH = 6.0) containing 10 mM $[Fe(CN)6]^{3-/4-}$(1:1) solution and 0.1 M KCl.

One-step green synthesis of polypyrrole-Au nanocomposite and its application in myoglobin aptasensor

Chong Sun[a], Daoying Wang[a,*], Zhiming Geng[a], Ling Gao[b], Muhan Zhang[a], Huan Bian[a], Fang Liu[a], Yongzhi Zhu[a], Haihong Wu[a], Weimin Xu[a,*]

[a]*Institute of Agricultural Products Processing, Jiangsu Academy of Agricultural Sciences, Nanjing 210014, China*

[b]*Jiangsu Collaborative Innovation Center of Biomedical Functional Materials, College of Chemistry and Materials Science, Nanjing Normal University, Nanjing 210023, China*

*Corresponding author.

E-mail address: daoyingwang@yahoo.com (D. Wang); weiminxu2002@aliyun.com (W. Xu)

Tel.: +86 25 84390065, Fax: +86 25 84390065

Graphical Abstract